Journal of Magnetic Resonance 301 (2019) 73–79

Contents lists available at ScienceDirect

Journal of Magnetic Resonance

journal homepage: www.elsevier.com/locate/jmr

Coil combination methods for multi-channel hyperpolarized ^{13}C imaging data from human studies

Zihan Zhu [a,b,*], Xucheng Zhu [a,b], Michael A. Ohliger [a], Shuyu Tang [a,b], Peng Cao [a], Lucas Carvajal [a], Adam W. Autry [a], Yan Li [a], John Kurhanewicz [a], Susan Chang [c], Rahul Aggarwal [c], Pamela Munster [c], Duan Xu [a], Peder E.Z. Larson [a], Daniel B. Vigneron [a], Jeremy W. Gordon [a]

[a] Department of Radiology and Biomedical Imaging, University of California, San Francisco, CA, United States
[b] UC Berkeley-UCSF Graduate Program in Bioengineering, University of California, San Francisco and University of California, Berkeley, CA, United States
[c] Department of Medicine, University of California, San Francisco, CA, United States

ARTICLE INFO

Article history:
Received 7 August 2018
Revised 19 January 2019
Accepted 30 January 2019
Available online 1 February 2019

Keywords:
Coil combination
^{13}C
Hyperpolarized
Pyruvate
DNP

ABSTRACT

Effective coil combination methods for human hyperpolarized ^{13}C spectroscopy multi-channel data had been relatively unexplored. This study implemented and tested several coil combination methods, including (1) the sum-of-squares (SOS), (2) singular value decomposition (SVD), (3) Roemer method by using reference peak area as a sensitivity map (RefPeak), and (4) Roemer method by using ESPIRiT-derived sensitivity map (ESPIRiT). These methods were evaluated by numerical simulation, thermal phantom experiments, and human cancer patient studies. Overall, the SVD, RefPeak, and ESPIRiT methods demonstrated better accuracy and robustness than the SOS method. Extracting complex pyruvate signal provides an easy and excellent approximation of the coil sensitivity map while maintaining valuable phase information of the coil-combined data.

1. Introduction

Initial human research studies have demonstrated both the safety and clinical potential of *in vivo* hyperpolarized (HP) ^{13}C molecular imaging [1–7]. HP ^{13}C-pyruvate MR metabolic imaging is being applied for identifying tumor metabolism [8], assessing aggressiveness [9], evaluating response to treatment [4,10], and probing cardiac function [3]. In these emerging applications, multichannel array coils can play a crucial role by providing large field-of-view (FOV) and volumetric coverage, and enabling parallel imaging acceleration [11].

Many coil combination methods have previously been proposed for multichannel proton (^{1}H) and phosphorous (^{31}P) MR applications [12–16]. There are generally three categories of coil combination methods: direct combination, data-driven combination, and using reference information for combination. With regard to direct combination, the most commonly used algorithm is sum-of-squares (SOS), with equal weight being given to each coil. The singular value decomposition (SVD) based methods [12,13] are examples of data-driven coil combinations. In addition, coil phases and weights have often been empirically estimated by calculating B_1^- [14] or by using a reference peak within the data in both imaging [17,18] and spectroscopic [15,16] applications.

In the field of hyperpolarized ^{13}C MRI, a number of published clinical and pre-clinical studies have used phased arrays for spectroscopic and imaging applications [2,3,19–26], and the choice of coil combination techniques varied between them, sometimes unspecified by authors. Among these studies, the SOS algorithm remains the most widely used and simplest method for combining multichannel data, despite lacking optimal SNR and its failure to preserve phase information. Notably departing from this common practice, Dominguez-Viqueira et al. [22] proposed using the Biot-Savart law and fiducial markers to numerically calculate the sensitivity estimates of each coil for hyperpolarized ^{13}C cardiac imaging applications. This analytical estimate of coil weights was shown to be an effective method of combining multichannel data, with only minor intrinsic limits of the Biot-Savart law, which neglects detailed factors such as coil loading and current distribution [22]. Lau et al. [23] have also proposed using the ESPIRiT method to estimate coil sensitivity maps for natural abundance ^{13}C phantom imaging, and Park et al. [2] have described using both the SOS algorithm and the hyperpolarized [1-^{13}C]pyruvate map to combine data for human brain imaging applications. Because coil

* Corresponding author at: Department of Radiology and Biomedical Imaging, University of California, San Francisco, 1700 Fourth Street, Byers Hall Suite 102, San Francisco, CA 94158, United States.
E-mail address: zihan.zhu.zz@gmail.com (Z. Zhu).

https://doi.org/10.1016/j.jmr.2019.01.015
1090-7807/

combination methods were not the central focus of these studies, the specific advantages and disadvantages were not evaluated in depth.

The accuracy and robustness of HP ^{13}C data quantification is important for translating this technique into clinical research, and for identifying optimal methods that will allow results to be standardized across study sites. The goal of this study was to investigate and evaluate four coil combination methods through simulation, phantom studies, and *in vivo* experiments, in order to develop a robust framework for multichannel clinical hyperpolarized ^{13}C spectroscopic and imaging data combination.

2. Methods

2.1. Coil combination theory

Four coil combination methods were evaluated in this study: (1) the sum-of-squares (SOS), (2) singular value decomposition (SVD) [13], (3) uniform noise Roemer method [11] by using reference peak area as a sensitivity map (RefPeak) [15], and (4) uniform noise Roemer method by using ESPIRiT [27]-derived sensitivity maps (ESPIRiT). The uniform noise Roemer method results in an SNR-optimal combination of multi-coil images [11].

Table 1 summarizes the methods and the key parameters used in this study. These methods are available from the Hyperpolarized MRI Toolbox via the Hyperpolarized Technology Resource Center training and dissemination website at: https://radiology.ucsf.edu/research/labs/hyperpolarized-mri-tech/training and https://github.com/LarsonLab/hyperpolarized-mri-toolbox.

2.2. Numerical simulations

Simulations were performed to evaluate the different coil combination methods. Coil combination methods were evaluated on a simulated single-voxel spectroscopy dataset. A spectrum with two resonances, representing lactate and pyruvate signals (lactate downfield and pyruvate upfield), was simulated for a 16-channel array by scaling the spectrum with 16 normalized and randomly generated complex scaling factors to create a phase shift. Different complex Gaussian noise with various standard deviations was added to each channel to create nominal peak pyruvate SNR between 14 and 283. The downfield resonance, simulating lactate, was designed to have 0.31 × Pyruvate SNR. Supplementary Fig. 1a shows the simulated 16-channel data with different sensitivity weighting and phase, and Supplementary Fig. 1b shows a representative dataset after adding noise to each channel with nominal peak pyruvate SNR of 57.

Four coil combination methods (ESPIRiT, RefPeak, SVD, and SOS) were applied to combine the spectra. Pyruvate was used as the reference peak for the RefPeak and ESPIRiT methods. After combining the multichannel coil data, the ratio of two peak areas (lactate-to-pyruvate ratio) was calculated by integrating the areas under each resonance of the magnitude spectra both with and without baseline subtraction. This process was repeated 200 times for each coil combination method at each noise level and the median and 25th–75th quartile of each method were displayed as a box plot. Statistical significance between the four coil combinations methods was assessed using a 1-way ANOVA corrected for multiple comparisons using Tukey's honest significance difference criterion.

2.3. Phantom experiment

All imaging studies were performed on a whole-body 3 T MRI scanner (MR750, GE Healthcare, Waukesha, WI, USA), with multi-nuclear excite and 32-channel receive capability.

For the phantom study, proton imaging was performed using the body coil for excitation and a 4-channel surface coil for reception. Carbon imaging was performed using a clamshell volume transmitter [25] and a 16-channel bilateral receive array (Rapid Biomedical, Rimpar, Germany). The anterior and posterior arrays, each housing 8 coil elements with a 4 × 2 layout, were placed above and below the phantom for whole volume coverage (Fig. 2f).

An abdominal-sized phantom containing natural abundance ethylene glycol and comprised of multiple signal voids was imaged by a ^{1}H T_2-weighted sequence and a ^{13}C spectroscopy sequence. The ^{13}C data were acquired from a 10 cm axial slice with an in-plane field-of-view (FOV) of 36 × 32 cm^2 (RL × AP) and in-plane resolution of 2.0 × 2.0 cm^2. An echo-planar spectroscopic imaging (EPSI) readout gradient was applied to encode one spatial (RL) dimension and the spectral dimension, with a readout bandwidth of 545 Hz and a spectral resolution of 10 Hz. 16 phase encodes were applied in the AP direction, and each was excited by a constant 90° sinc pulse with TR/TE = 312/3.5 ms. A total of 5 signal averages were acquired, resulting in a 25-second scan time.

Table 1
Summary of coil combination methods with spectroscopy and imaging applications.

	Spectroscopy application	Imaging application
SOS	$I_{SOS}\left(x_i,y_j,f\right)=\sqrt{\sum_k^{K_{Coil}}\left\|I(x_i,y_j,f,c_k)\right\|^2}$	$I_{SOS}\left(x_i,y_j,N\right)=\sqrt{\sum_k^{K_{Coil}}\left\|I(x_i,y_j,N,c_k)\right\|^2}$
SVD	$U\times\Sigma\times V^H=SVD\left(I\left(x_i,y_j,f,c\right)\right)$ $\sigma_1=\max(\Sigma)$ u_1=$U_{:,1}$ $I_{SVD}\left(x_i,y_j,f\right)=\sigma_1 u_1\varnothing$	N/A
RefPeak	$S\left(x_i,y_j,c_k\right)=\frac{I\left(x_i,y_j,f_{Ref},c_k\right)}{I_{SOS}\left(x_i,y_j,f_{Ref}\right)}$ $I_{RefPeak}\left(x_i,y_j,f\right)=\sum_k^{K_{Coil}}S^*\left(x_i,y_j,c_k\right)I(x_i,y_j,f,c_k)$	$S\left(x_i,y_j,c_k\right)=\frac{I\left(x_i,y_j,N_{Ref},c_k\right)}{I_{Ref_S OS}\left(x_i,y_j,N_{Ref}\right)}$ $I_{RefPeak}\left(x_i,y_j,N\right)=\sum_k^{K_{Coil}}S^*\left(x_i,y_j,c_k\right)I(x_i,y_j,N,c_k)$
ESPIRiT	$S\left(x_i,y_j,c_k\right)=Ecalib(ksp_{calib})$ $I_{ESPIRiT}\left(x_i,y_j,f\right)=\sum_k^{K_{Coil}}S^*\left(x_i,y_j,c_k\right)I(x_i,y_j,f,c_k)$	$S\left(x_i,y_j,c_k\right)=Ecalib(ksp_{calib})$ $I_{ESPIRiT}\left(x_i,y_j,N\right)=\sum_k^{K_{Coil}}S^*\left(x_i,y_j,c_k\right)I(x_i,y_j,N,c_k)$

I: original data; x_i: ith voxel in one spatial dimension; y_j: jth voxel in the other spatial dimension; f: spectral points; c_k and K: kth channel with a total of K channels; N: metabolite in metabolite-specific imaging approach; ∅: arbitrary phase for each voxel; S: sensitivity map; *: conjugate; H: conjugate transpose.
f_{Ref}: reference peak picked from spectroscopic datasets for coil combination.
N_{Ref}: reference metabolite image used for imaging datasets coil combination.
ksp_{calib}: part of k-space data used for ESPIRiT-derived sensitivity map calculation.
I_{SOS}, I_{SVD}, $I_{RefPeak}$, $I_{ESPIRiT}$: combined spectroscopy or imaging datasets with the SOS, SVD, RefPeak, and ESPIRiT methods.

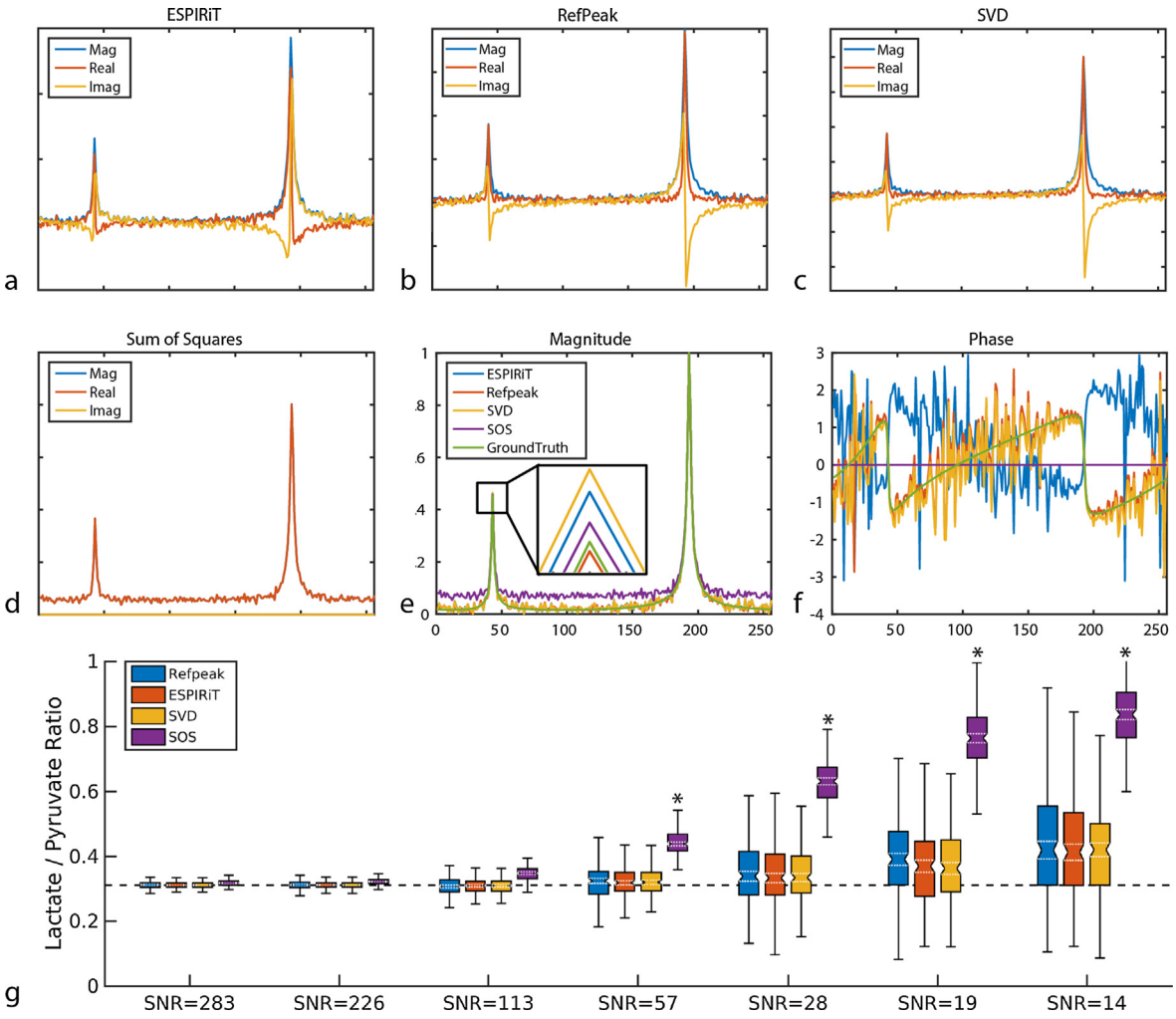

Fig. 1. Simulated single-voxel spectroscopic data combined by (a) ESPIRiT method, (b) RefPeak method, (c) SVD method, and (d) SOS method at a representative noise with nominal pyruvate SNR of 57. (e) and (f) The normalized magnitude spectra and spectral phase compared to simulation ground truth. Lactate-to-pyruvate ratio without baseline subtraction (g) was quantified for each coil combination method as a function of pyruvate SNR. Each box encloses the 25th–75th percentile, while the ground truth is denoted by the dashed black line. For simplicity outliers are not shown. Note the overestimation of the SOS reconstruction, even at high SNR. Simulation results with baseline subtraction can be found in Supplementary Fig. 2. *Denotes significant difference ($p < 0.05$) from the ground truth.

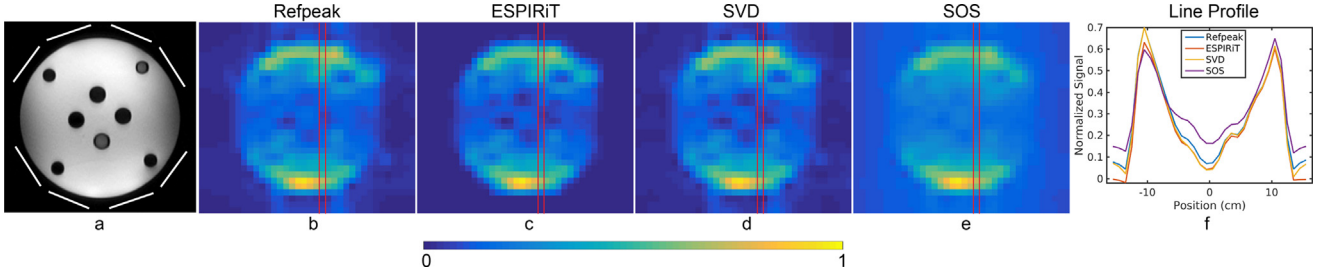

Fig. 2. Ethylene glycol phantom (a) results acquired by a ^{13}C spectroscopic imaging sequence using a clamshell transmitter and a 16-channel receive array. (b)–(e) The four coil combination results as images after integrating the central peak of ethylene glycol. (f) The line profile of the column highlighted in red in images (b)–(e). Note the elevated noise level in the SOS image and increased contrast and conspicuity of signal voids at the center of the phantom in the three data-driven (ESPIRiT, RefPeak, and SVD) methods. Reconstructed images have been zerofilled two-fold and displayed on the same normalized scale. (For interpretation of the references to colour in this figure legend, the reader is referred to the web version of this article.)

2.4. Hyperpolarization

A 1.43 g sample of [1-^{13}C] pyruvic acid (Millipore-Sigma, Miamisburg, OH) mixed with 28 mg of trityl radical (GE Healthcare, Oslo, Norway) was pre-filled in a plastic fluid path, and polarized for at least 2 h in a SPINlab system (General Electric, Niskayuna, NY), which operated at 5 T and 0.77 Kelvin with 140 GHz microwave irradiation. Sterile water was used for dissolution, and followed by the filtering, neutralizing, and diluting process. Following quality control system testing and pharmacist

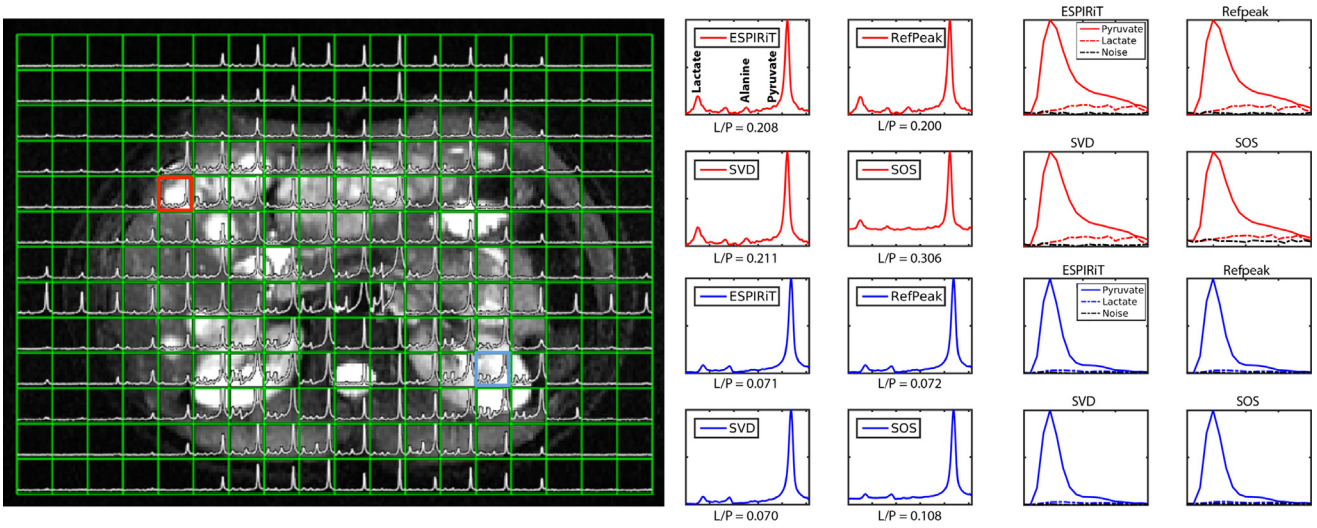

Fig. 3. Human HP ^{13}C 16-channel spectroscopic data registered to a ^{1}H T_2-weighted image, acquired from a breast cancer patient with liver metastases. The red box and red spectra correspond to a tumor voxel, whlie the blue box and blue spectra correspond to a kidney voxel. Pyruvate signal outside of the abdomen is due to respiratory motion during the 60 s free breathing scan. Lactate-to-pyruvate ratio (L/P) was quantified and displayed next to each coil-combined spectrum along with the dynamic pyruvate and lactate signal over the 60 s time course. ^{1}H T_2-weighted data were acquired with a Single Shot Fast Spin Echo (SSFSE) sequence with fat saturation. (For interpretation of the references to colour in this figure legend, the reader is referred to the web version of this article.)

approval, 0.43 mL/kg of the dissolved pyruvate solution (250 mM) followed by 20 mL of sterile saline were injected intravenously at a rate of 5 mL/s using a power injector (MEDRAD, Inc).

2.5. Patient studies

All human studies followed an IRB and FDA IND-approved protocol with informed consent.

A breast cancer patient with metastases to the liver was imaged using a standard clinical liver imaging protocol and a 2D dynamic ^{13}C EPSI sequence. The 16-channel coil setup was similar to the phantom experiment, and the two ^{13}C receiver arrays were placed anterior and posterior to the patient's abdomen. The HP ^{13}C imaging parameters were as follows: multiband spectral-spatial RF pulse with 10° excitation on pyruvate and 20° excitation on lactate within a 2 cm axial slab, TR/TE was 130/3.5 ms, 3 s temporal resolution with 20 total time frames, 16 phase encodes in AP direction, a symmetric EPSI readout in the RL direction, and an in-plane resolution of 1.8 cm × 1.8 cm. The EPSI readout bandwidth was 545 Hz and with a spectral resolution of 10 Hz.

A treated brain patient volunteer was imaged post-surgery using a custom-built 32-channel ^{13}C coil [28]. Volumetric data were acquired with a metabolite-specific EPI sequence [29] using a spectral-spatial RF pulse (130 Hz FWHM, 868 Hz stopband peak-to-peak). Eight 2 cm slices were acquired with a 24 × 24 cm^2 FOV, 16 × 16 matrix, (1.5 × 1.5 cm^2 in-plane resolution), 62.5 ms TR, 21.7 ms TE, 20 kHz BW, and 1.03 ms echo-spacing. The center frequency was alternated between [1-^{13}C] pyruvate (Δf = 0 Hz), [1-^{13}C] lactate (Δf = 390 Hz) and ^{13}C bicarbonate (Δf = −320 Hz) to independently encode each metabolite volume, and a 1.5 s delay was inserted after the bicarbonate volume to yield a 3 s temporal resolution. Twenty total timeframes per metabolite were acquired, yielding a total imaging time of 60 s.

2.6. Data analysis

All ^{13}C spectroscopic imaging data were processed in MATLAB (The MathWorks Inc., Natick, MA). A 2D dynamic spectroscopic dataset was reconstructed after zero-filling the free induction decays (FIDs) to 256 points, apodizing with a 10-Hz Gaussian filter, re-sampling to create a uniform data grid, pre-whitening [30], and then applying Fourier transformation.

The four coil combination methods were each applied to the phantom and human HP ^{13}C datasets to compare performance. For the phantom experiment, the summed center peak ethylene glycol triplet served as the reference peak for the RefPeak and ESPIRiT methods. After coil combination using the four methods in the spectral domain, each method was displayed as an image by summing the magnitude spectral region of the center peak of the ethylene glycol triplet, as shown in Fig. 2a–d, for direct image comparison. For the human HP ^{13}C spectroscopic dataset, the summed pyruvate peak was integrated as the reference peak for these two coil combination methods.

^{13}C EPI data were processed using the Orchestra reconstruction toolbox (GE Healthcare). Data were first corrected for Nyquist ghost artifacts by choosing the appropriate phase coefficients via an exhaustive search [31] and then pre-whitened in k-space prior to coil combination. Due to the nature of imaging approaches, the SVD method was not applicable since spectral selection was performed during excitation. Three methods, ESPIRiT, RefPeak, and SOS, were applied to the multi-channel imaging data. Three metabolites, pyruvate, lactate, and bicarbonate, from the 4 central slices were displayed for each method, as shown in Fig. 4. In Fig. 5, the lactate-to-pyruvate ratio and bicarbonate-to-pyruvate ratio maps were generated after thresholding by pyruvate SNR, along with scatter plots of the ratios by the three coil combination methods.

The Berkeley Advanced Reconstruction Toolbox (BART) [32] was used for ESPIRiT reconstruction. The same ESPIRiT parameters were used for all datasets as follows: kernel size of 4, calibration region of 8, soft SENSE, eigenvalue threshold of 0.9.

3. Results

Computer simulation demonstrated the performance of each of the four coil combination methods at different noise levels in the case of a single voxel spectroscopy dataset, as shown in Fig. 1. Fig. 1a–d shows a representative dataset with a pyruvate SNR of 57 reconstructed with different coil combination methods. After normalizing each magnitude spectrum to pyruvate, only minor differences could be observed in terms of lactate peak magnitude

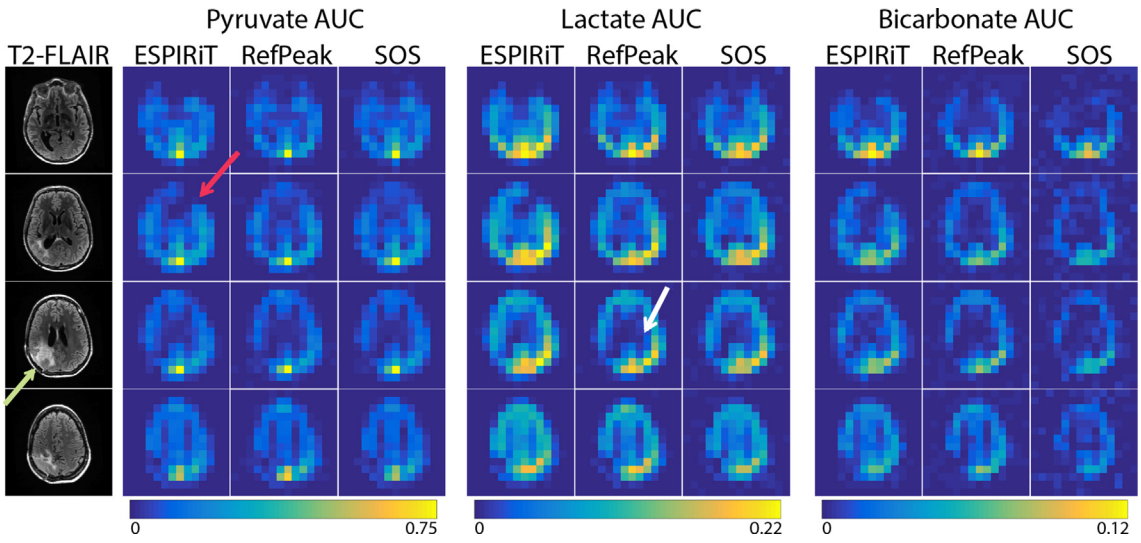

Fig. 4. Brain patient data with ^{1}H T_2-FLAIR images (treated lesion post-resection indicated by the green arrow) and AUC images acquired with EPI of three metabolites using a 32-channel ^{13}C coil. Metabolite maps are shown on a normalized scale, with each reconstruction normalized to the maximum pyruvate signal. The white arrow highlights the different lateral ventricle contrast shown with the RefPeak method, while the red arrow points out a region with nulled signal by the ESPIRiT reconstruction, a result of the sensitivity map estimation. (For interpretation of the references to colour in this figure legend, the reader is referred to the web version of this article.)

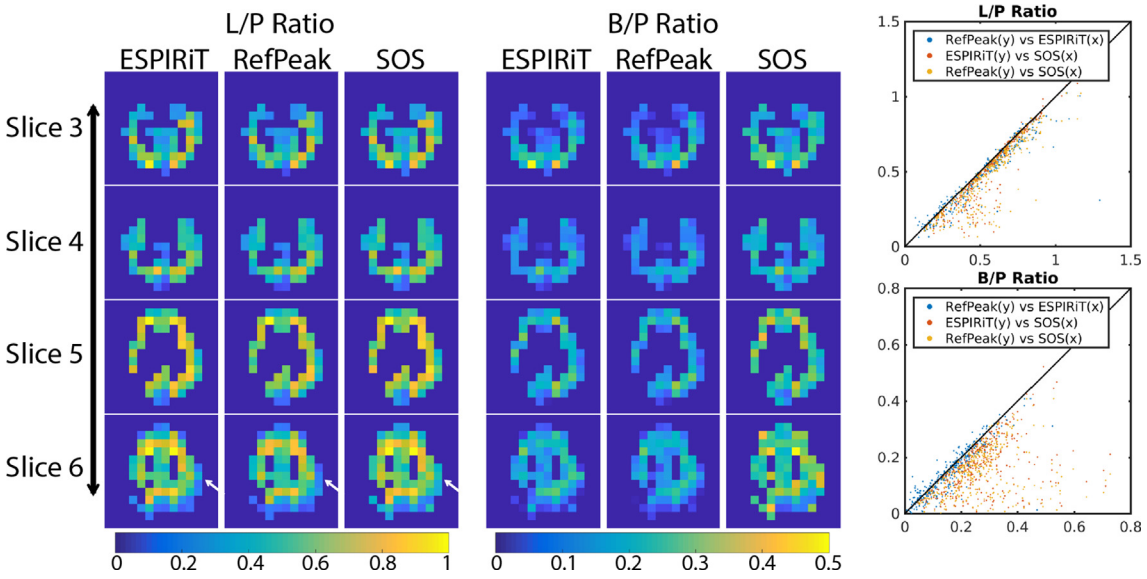

Fig. 5. Quantified lactate-to-pyruvate and bicarbonate-to-pyruvate ratios (L/P and B/P) of each voxel were plotted as scatter plots to compare three coil combination methods. The diagonal black line represents complete agreement between the methods. The masks were selected based on pyruvate SNR (voxels with SNR greater than 10) on a slice-by-slice basis, with the same mask applied to all three metabolite images. The white arrows indicate minor differences between the lactate-to-pyruvate ratio maps. Scatterplots on the right show good agreement between the RefPeak and ESPIRiT coil combination methods, while the SOS method tends to overestimate the ratio when SNR is low, in agreement with simulation results.

among different coil combination methods, as shown in Fig. 1e. In addition, the SOS method showed an elevated spectral baseline compared to the ground truth. Fig. 1f shows the phase of the ground truth spectrum and the coil-combined spectra. In this representative case, the ESPIRiT, RefPeak, and SVD methods preserved the phase well compared to the ground truth, whereas the SOS method completely lost such information as expected.

After repeating each coil combination method 200 times at 7 different SNR levels, the non baseline-subtracted (Fig. 1g) lactate-to-pyruvate ratio median and 25th–75th percentiles of each method were plotted. For the non baseline subtracted ratios, all four methods performed very similarly and accurately when pyruvate SNR was higher than 100, with <15% error from the ground truth. However, there was significant overestimation ($p < 0.05$) in the lactate-to-pyruvate ratio at SNR $\leq$ 57 for the SOS method. At an SNR of 19, the SOS method was the least robust to noise and overestimated the lactate-to-pyruvate ratio by 180%, while the ESPIRiT, RefPeak, and SVD methods had lower bias and overestimated the ratio by roughly 30%. In contrast, the baseline subtracted ratios (Supplementary Fig. 2g) were consistently and significantly ($p < 0.05$) underestimated by the SOS reconstruction, even at high SNR levels. There was no significant difference in the lactate-to-pyruvate ratio for either of the three data-driven approaches at any SNR level explored in this work.

The spectroscopic phantom data was coil combined by the four methods in the spectral dimension and displayed in Fig. 2b–e as images by integrating the center peak of the ethylene glycol triplet and normalizing to the maximum pixel. The line profile of the

same column of each image was plotted in Fig. 2f. Overall, the ESPIRiT method was the best at suppressing the background noise, while the three data-driven methods (ESPIRiT, RefPeak, and SVD) performed similarly under different noise levels throughout the phantom. Consistent with the simulation results, the SOS method tended to overestimate the signal at high noise regions, and the background noise was elevated compared to the other methods. This is most evident at the center of the phantom, where the elevated noise reduces the contrast and conspicuity of the signal voids in the SOS image.

The human HP ^{13}C spectroscopic data provided similar results as the simulation and phantom experiments. Fig. 3 shows the ^{13}C spectroscopic data overlaid on top of a T_2-weighted ^{1}H image, the four coil-combined spectra of a tumor voxel and a kidney voxel, and the respective dynamic time course for pyruvate and lactate. Supplementary Fig. 3 shows the same data but analyzed with baseline subtracted spectra. In the tumor voxel, four peaks (lactate, pyruvate hydrate, alanine, and pyruvate) could be observed. Qualitatively, the ESPIRiT, RefPeak, and SVD methods performed similarly, whereas the SOS method showed elevated spectral baseline and posed more deteriorating effects on low SNR peaks such as alanine. In the kidney voxel, only three peaks were observed, lactate, pyruvate hydrate, and pyruvate, and the relative difference among the coil combination methods were similar to that of the tumor voxel. The kidney voxel lactate-to-pyruvate ratio was quantified by dividing the summed magnitude spectra regions of the two metabolites, and ESPIRiT and RefPeak methods provided the same ratio quantification, while the SVD method showed slightly lower ratios and the SOS method overestimated ratios due to an elevated baseline.

Only three coil combination methods were evaluated using the HP ^{13}C EPI data, and the images of each metabolite are shown in Fig. 4. The image from pyruvate was taken as representative of the high SNR case, while the downstream metabolites, lactate and bicarbonate, were representative of the moderate and low SNR situations. In the high SNR case, the pyruvate images from the three coil combinations were similar, except the ESPIRiT method demonstrated a signal null in the left frontal lobe, as indicated by the red arrow in Fig. 4 (this nulled region could be observed in ESPIRiT images of lactate and bicarbonate as well). This was due to the choice of high eigenvalue threshold of the ESPIRiT parameters, and it could potentially be avoided by fine-tuning the ESPIRiT input. The green arrow indicates the region of the patient's surgical resection, and showed low levels of ^{13}C signal, consistent with low blood perfusion. From the lactate images, which represented a moderate SNR case, better lateral ventricle contrast could be observed from the RefPeak method, as pointed out by the white arrow. Both ESPIRiT and RefPeak methods outperformed the SOS method in the low SNR bicarbonate images, showing better image SNR and contrast. All three metabolites had the highest SNR towards the posterior, reflecting the sensitivity profile of the 32-channel array. Ratio maps of lactate-to-pyruvate and bicarbonate-to-pyruvate of each method were displayed in Fig. 5, along with scatter plots of the ratios by different methods. The three methods showed similar lactate-to-pyruvate ratios, in agreement with simulations indicating minimal difference between approaches at moderate-to-high SNR. However, the low SNR bicarbonate-to-pyruvate ratio showed more scatter when the two data-driven approaches were compared to the SOS method. Consistent with simulation, the SOS method overestimated the ratios in low SNR cases when compared to the two data-driven methods.

4. Discussion

The computer simulation, phantom testing, and human *in vivo* experimental data in this project comparing multi-channel combination methods all provided consistent results at high SNR. Among the four coil combination methods being evaluated in this study, the SOS method was the most straightforward and easy to compute, but showed the worst results, while the other three methods (ESPIRiT, SVD, and RefPeak) all performed similarly.

For spectroscopic reconstruction, the SOS method did not preserve phase information (as expected), while the other three methods all used the pyruvate phase of each voxel as reference phase. This phase correction step was intrinsic to the RefPeak method, as phase was preserved as complex coil weights. Phase correction was performed for ESPIRiT and SVD methods after coil combination, by applying constant spectral phase of a non-noise reference point on a voxel-by-voxel based operation. All three methods will be prone to phase errors for low SNR voxels, thus consideration must be given for phase-sensitive and SNR-limited acquisitions.

The SOS method showed the least desirable results for both spectroscopy and imaging applications. This method was more prone to error in terms of metabolite ratio quantifications, since low SNR signals were contaminated by elevated bias leading to overestimated ratios in data without baseline subtraction and underestimated ratios with baseline subtraction. Lactate-to-pyruvate and bicarbonate-to-pyruvate ratios tended to be overestimated by the SOS method in the low SNR voxels. In addition to the quantification advantage, the RefPeak, SVD, and ESPIRiT methods all showed greatly enhanced apparent SNR, especially for metabolites with relatively low intrinsic concentration such as bicarbonate and alanine. Compared to the SOS coil combination method, the RefPeak, SVD, and ESPIRiT also enhanced image and spectral quality of dynamic data, which will enable robust quantification of the HP ^{13}C metabolites.

The coil shading observed in the reconstructed images is an outcome of the coil sensitivities estimated from the *in vivo* data. In a data-driven (or self-calibrated) reconstruction, the coil sensitivities are not 'absolute' but rather are a product of the true coil sensitivities and the underlying spin density of the reference peak, which was pyruvate in this work. An absolute sensitivity measurement generally requires the use of a body coil reference, which is not usually available for carbon-13 acquisitions. A downside of these data-driven coil combination approaches is that the final images remain modulated by the sum-of-squares coil sensitivity profile.

In this study, all phantom and *in vivo* data were pre-whitened prior to the rest of reconstruction. This pre-whitening step removed the noise correlations between channels and scaled the noise to identical amplitudes. Pre-whitening has been previously shown to provide significant benefits in terms of precision and efficiency [13], and should be considered as a routine pre-processing step for multi-channel HP ^{13}C data reconstruction.

While the RefPeak and ESPIRiT methods performed similarly in simulation, there were subtle differences in the coil-combined images. This was primarily due to the coil sensitivity estimation and is related to the eigenvalue threshold chosen in the reconstruction. Care must be taken when choosing parameters for the ESPIRiT method during the sensitivity map calculation. Fine-tuning the ESPIRiT parameters could potentially improve the results but could also cause risk biased and misleading results. As demonstrated in Fig. 4 by the red arrow, the thresholding step mistakenly removed signal from areas with low signal profile. In this, the RefPeak method is more advantageous due to its input-less nature.

5. Conclusions

In this study, we have developed a framework for comparing different reconstructions of multi-channel hyperpolarized ^{13}C MR data. The three data-driven coil combination methods explored in this work (ESPIRiT, SVD, and RefPeak) had improved performance and accuracy when compared to a conventional

sum-of-squares combination. Of these approaches, the RefPeak method is appealing since the complex pyruvate signal provides an input-less approximation of the relative coil sensitivities, maintains the phase information, and is compatible with both imaging and spectroscopic applications.

Acknowledgement

This work was supported by NIH grants R01CA183071 and P41EB013598. The authors would like to acknowledge Jennifer Chow, Romelyn Delos Santos, Kimberley Okamoto, Mary McPolin, Hope Williams, James B. Slater, and Patrick Koon for their help with the human studies.

Appendix A. Supplementary material

Supplementary data to this article can be found online at https://doi.org/10.1016/j.jmr.2019.01.015.

References

[1] S.J. Nelson, J. Kurhanewicz, D.B. Vigneron, et al., Metabolic imaging of patients with prostate cancer using hyperpolarized [1-13C] pyruvate, Sci. Transl. Med. 5 (198) (2013) 198ra108, https://doi.org/10.1126/scitranslmed.3006070.
[2] I. Park, P.E.Z. Larson, J.W. Gordon, et al., Development of methods and feasibility of using hyperpolarized carbon-13 imaging data for evaluating brain metabolism in patient studies, Magn. Reson. Med. 80 (3) (2018) 864–873, https://doi.org/10.1002/mrm.27077.
[3] C.H. Cunningham, J.Y.C. Lau, A.P. Chen, et al., Hyperpolarized 13C metabolic MRI of the human heart, Circ. Res. (2016) 1177–1183, https://doi.org/10.1161/CIRCRESAHA.116.309769.
[4] R. Aggarwal, D.B. Vigneron, J. Kurhanewicz, Hyperpolarized 1-[13C]-pyruvate magnetic resonance imaging detects an early metabolic response to androgen ablation therapy in prostate cancer, Eur. Urol. 72 (6) (2017) 1028–1029, https://doi.org/10.1016/j.eururo.2017.07.022.
[5] H.-Y. Chen, P.E.Z. Larson, J.W. Gordon, et al., Technique development of 3D dynamic CS-EPSI for hyperpolarized 13 C pyruvate MR molecular imaging of human prostate cancer, Magn. Reson. Med. (2018), https://doi.org/10.1002/mrm.27179.
[6] J.W. Gordon, R.B. Hansen, P.J. Shin, Y. Feng, D.B. Vigneron, P.E.Z. Larson, 3D hyperpolarized C-13 EPI with calibrationless parallel imaging, J. Magn. Reson. 2018 (289) (2018) 92–99, https://doi.org/10.1016/j.jmr.2018.02.011.
[7] V.Z. Miloushev, K.L. Granlund, R. Boltyanskiy, et al., Metabolic imaging of the human brain with hyperpolarized 13C pyruvate demonstrates 13C lactate production in brain tumor patients, Cancer Res. (2018), https://doi.org/10.1158/0008-5472.CAN-18-0221.
[8] K. Golman, R.i. Zandt, M. Lerche, R. Pehrson, J.H. Ardenkjaer-Larsen, Metabolic imaging by hyperpolarized 13C magnetic resonance imaging for in vivo tumor diagnosis, Cancer Res. 66 (22) (2006) 10855–10860, https://doi.org/10.1158/0008-5472.CAN-06-2564.
[9] H. Chen, P.E.Z. Larson, R.A. Bok, et al., Assessing Prostate Cancer Aggressiveness with Hyperpolarized Dual-Agent 3D Dynamic Imaging of Metabolism and Perfusion, Cancer Res. 77 (12) (2017) 3207–3217, https://doi.org/10.1158/0008-5472.CAN-16-2083.
[10] S.E. Day, M.I. Kettunen, F.a. Gallagher, et al., Detecting tumor response to treatment using hyperpolarized 13C magnetic resonance imaging and spectroscopy, Nat. Med. 13 (11) (2007) 1382–1387, https://doi.org/10.1038/nm1650.
[11] P.B. Roemer, W.A. Edelstein, C.E. Hayes, The NMR phased array, Magn Reson Med. 16 (1990) 192–225.
[12] N. Sandgren, P. Stoica, F.J. Frigo, Y. Selen, Spectral analysis of multichannel MRS data, J. Magn. Reson. 175 (1) (2005) 79–91, https://doi.org/10.1016/j.jmr.2005.03.019.
[13] C.T. Rodgers, M.D. Robson, Receive array magnetic resonance spectroscopy: whitened singular value decomposition (WSVD) gives optimal bayesian solution, Magn. Reson. Med. 63 (4) (2010) 881–891, https://doi.org/10.1002/mrm.22230.
[14] C.T. Rodgers, M.D. Robson, Coil combination for receive array spectroscopy: are data-driven methods superior to methods using computed field maps?, Magn Reson. Med. 75 (2) (2016) 473–487, https://doi.org/10.1002/mrm.25618.
[15] E.L. Hall, M.C. Stephenson, D. Price, P.G. Morris, Methodology for improved detection of low concentration metabolites in MRS: optimised combination of signals from multi-element coil arrays, Neuroimage 2014 (86) (2014) 35–42, https://doi.org/10.1016/j.neuroimage.2013.04.077.
[16] L. An, J.W. Van Der Veen, S. Li, D.M. Thomasson, J. Shen, Combination of multichannel single-voxel MRS signals using generalized least squares, J. Magn. Reson. Imag. 37 (6) (2013) 1445–1450, https://doi.org/10.1002/jmri.23941.
[17] C.A. Mckenzie, M.A. Ohliger, E.N. Yeh, M.D. Price, D.K. Sodickson, Coil-by-coil image reconstruction with SMASH, Magn Reson Med. 46 (3) (2001) 619–623.
[18] C.A. Mckenzie, E.N. Yeh, M.A. Ohliger, M.D. Price, D.K. Sodickson, Self-Calibrating Parallel Imaging With Automatic Coil Sensitivity Extraction, Magn Reson Med. 47 (3) (2002) 529–538, https://doi.org/10.1002/mrm.10087.
[19] E.S.S. Hansen, R.S. Tougaard, T.S. Nørlinger, et al., Imaging Porcine Cardiac Substrate Selection Modulations by Glucose, Insulin and Potassium Intervention: A Hyperpolarized [1-^{13}C] Pyruvate Study, NMR Biomed. 30 (6) (2017), https://doi.org/10.1002/nbm.3702 e3702.
[20] R. Schmidt, C. Laustsen, J. Dumez, et al., In vivo single-shot 13 C spectroscopic imaging of hyperpolarized metabolites by spatiotemporal encoding, J. Magn. Reson. 2014 (240) (2014) 8–15, https://doi.org/10.1016/j.jmr.2013.12.013.
[21] E.S.S. Hansen, N.J. Stewart, J.M. Wild, Stødkilde-jørgensen H, Laustsen C. Hyperpolarized 13C,15N2-Urea MRI for assessment of the urea gradient in the porcine kidney, Magn. Reson. Med. (2016) 1895–1899, https://doi.org/10.1002/mrm.26483.
[22] W. Dominguez-viqueira, B.J. Geraghty, J.Y.C. Lau, F.J. Robb, A.P. Chen, C.H. Cunningham, Intensity correction for multichannel hyperpolarized C imaging of the heart, Magn. Reson. Med. 78 (2016) 859–865, https://doi.org/10.1002/mrm.26042.
[23] A.Z. Lau, J.Y.C. Lau, A.P. Chen, C.H. Cunningham, Simultaneous multislice acquisition without trajectory modification for hyperpolarized 13C experiments, Magn Reson Med. 80 (4) (2018) 1588–1594, https://doi.org/10.1002/mrm.27136.
[24] A. Arunachalam, D. Whitt, K. Fish, et al., Accelerated spectroscopic imaging of hyperpolarized C-13 pyruvate using SENSE parallel imaging, NMR Biomed. 22 (8) (2009) 867–873, https://doi.org/10.1002/nbm.1401.
[25] J. Tropp, J.M. Lupo, A. Chen, et al., Multi-channel metabolic imaging, with SENSE reconstruction, of hyperpolarized [1-(13)C] pyruvate in a live rat at 3.0 tesla on a clinical MR scanner, J. Magn. Reson. 208 (1) (2011) 171–177, https://doi.org/10.1016/j.jmr.2010.10.007.
[26] M.a. Ohliger, P.E.Z. Larson, R.A. Bok, et al., Combined parallel and partial fourier MR reconstruction for accelerated 8-channel hyperpolarized carbon-13 in vivo magnetic resonance Spectroscopic imaging (MRSI), J. Magn. Reson. Imag. 38 (3) (2013) 701–713, https://doi.org/10.1002/jmri.23989.
[27] M. Uecker, P. Lai, M.J. Murphy, et al., ESPIRiT — An Eigenvalue Approach to Autocalibrating Parallel MRI : Where SENSE Meets GRAPPA, Magn Reson Med. 71 (3) (2014) 990–1001, https://doi.org/10.1002/mrm.24751.
[28] A. areyam, L. Carvajal, D. Xu et al., 31-Channel brain array for hyperpolarized ^{13}C imaging at 3T. In: Proceedings of the 25th Annual Meeting of ISMRM, 2017. pp. 1225.
[29] J.W. Gordon, D.B. Vigneron, P.E.Z. Larson, Development of a symmetric echo planar imaging framework for clinical translation of rapid dynamic hyperpolarized 13C imaging, Magn. Reson. Med. 77 (2) (2017) 826–832, https://doi.org/10.1002/mrm.26123.
[30] P. Kellman, E.R. Mcveigh, Image Reconstruction in SNR Units: A General Method for SNR, Measurement 54 (6) (2005) 1439–1447, https://doi.org/10.1002/mrm.20713.
[31] J. Wang, A.J. Wright, R.L. Hesketh, D.E. Hu, K.M. Brindle, A referenceless Nyquist ghost correction workflow for echo planar imaging of hyperpolarized [1-13C]pyruvate and [1-13C]lactate, NMR Biomed. 31 (2) (2018) 1–13, https://doi.org/10.1002/nbm.3866.
[32] M. Uecker, F. Ong, J.I. Tamir, et al., Berkeley advanced reconstruction toolbox, in: Proc 23rd Annu Meet ISMRM. 2015, 2015, p. 2486, https://doi.org/10.1002/mrm.25176.